

## The X 1 $\Sigma$ g + ground state of Mg<sub>2</sub> studied by Fourier-transform spectroscopy

H. Knöckel, S. Rühmann, and E. Tiemann

Citation: *The Journal of Chemical Physics* **138**, 094303 (2013); doi: 10.1063/1.4792725

View online: <http://dx.doi.org/10.1063/1.4792725>

View Table of Contents: <http://scitation.aip.org/content/aip/journal/jcp/138/9?ver=pdfcov>

Published by the [AIP Publishing](#)

---

### Articles you may be interested in

[Extended Fourier-transform spectroscopy studies and deperturbation analysis of the spin-orbit coupled A 1 \$\Sigma\$ + and b 3 \$\Pi\$  states in RbCs](#)

*J. Chem. Phys.* **141**, 184309 (2014); 10.1063/1.4901327

[Erratum: "The X 1  \$\Sigma\$  g + ground state of Mg<sub>2</sub> studied by Fourier-transform spectroscopy" \[\*J. Chem. Phys.\* 138, 094303 \(2013\)\]](#)

*J. Chem. Phys.* **138**, 189901 (2013); 10.1063/1.4804611

[Fourier transform spectroscopy and direct potential fit of a shelflike state: Application to E\(4\)1 \$\Sigma\$ + KCs](#)

*J. Chem. Phys.* **134**, 104307 (2011); 10.1063/1.3561318

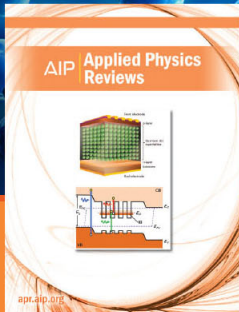
[High-resolution studies of tropolone in the S 0 and S 1 electronic states: Isotope driven dynamics in the zero-point energy levels](#)

*J. Chem. Phys.* **124**, 074309 (2006); 10.1063/1.2165652

[Characterization of the CCCI radical in the X 2 A ' state by Fourier-transform microwave spectroscopy and ab initio calculations](#)

*J. Chem. Phys.* **119**, 1426 (2003); 10.1063/1.1581851

---



**NEW Special Topic Sections**

**NOW ONLINE**  
Lithium Niobate Properties and Applications:  
Reviews of Emerging Trends

**AIP** | Applied Physics  
Reviews

# The $X^1\Sigma_g^+$ ground state of $Mg_2$ studied by Fourier-transform spectroscopy

H. Knöckel, S. Rühmann, and E. Tiemann

*Institute for Quantum Optics, Leibniz Universität Hannover, Welfengarten 1, 30167 Hannover, Germany*

(Received 8 January 2013; accepted 6 February 2013; published online 1 March 2013)

The  $A^1\Sigma_u^+ - X^1\Sigma_g^+$  UV spectrum of  $Mg_2$  has been investigated with high resolution Fourier-transform spectroscopy.  $Mg_2$  vapor was created in a heat pipe. Various spectroscopic methods have been employed, such as conventional absorption spectroscopy with light from a broad band lamp and laser-induced fluorescence. The high resolution of the Fourier-transform spectrometer, together with computer aided evaluation methods of the spectra, yields precise transition frequencies. The new data and data available from earlier investigations are applied in direct potential fits of lower and upper electronic states. Various representations of potential energy curves for the ground state  $X^1\Sigma_g^+$  have been employed and their benefits in terms of smallest number of parameters are discussed. Scattering lengths are derived for the homonuclear isotopologues and compared with previous results. © 2013 American Institute of Physics. [<http://dx.doi.org/10.1063/1.4792725>]

## I. INTRODUCTION

Currently, a strong interest in the cooling and trapping of alkaline earth metal atoms and electronically similar species such as Yb or Hg exists. Recently, Bose-Einstein condensation was obtained for Ca,<sup>1</sup> Sr,<sup>2</sup> and Yb.<sup>3</sup> On the other hand, alkaline earth atoms are important regarding perspectives for ultra stable optical clocks, as they provide extremely narrow optical transitions between their ground state  $^1S$  and the  $^3P$  multiplet. While mostly Sr and Ca have been under consideration, also Mg has been investigated for its suitability for an optical frequency standard (see Ref. 4 and references therein) in the blue spectral range.

The main isotopes of alkaline earth atoms have nuclear spin zero, so they have no hyperfine structure and thus exhibit much simpler spectral structure than, e.g., alkali atoms. For full quantitative understanding of cold collision properties of ultracold atoms and for proposing production schemes of ultracold molecules, it is necessary to know interatomic potentials from long range down to small internuclear distances around the binding part of a potential well and even the repulsive branch. This range can be investigated by molecular spectroscopy of the corresponding diatomic molecules. For  $Ca_2$  and  $Sr_2$ , we have characterized the ground states<sup>5,6</sup> and some of the lowest excited electronic states.<sup>7,8</sup> In those examples, it also became obvious, that present *ab initio* calculations of the electronic structure of these diatomic alkaline earth molecules do not describe the experimentally found electronic structure as precisely as it is known, e.g., from the case of alkali dimers.

Highly reliable calculations are important regarding creation of ultracold molecules from ultracold atomic samples. A common synthesis employed for diatomic alkalis uses the photoassociation of molecules with laser light, where colliding cold atoms are excited into a bound molecular state, from which they are either transferred by spontaneous decay or by induced transitions to levels of the ground state.<sup>9</sup> Also, coherent stimulated Raman adiabatic passage (STIRAP) processes are applied to create cold ground state molecules starting from a magnetically associated,

weakly bound Feshbach molecule (see, e.g., Ref. 10). The spontaneous formation of molecules from colliding atoms in the presence of light seems to work exceptionally well with alkaline earth species. Already as early as 1977 Scheingraber *et al.*<sup>11</sup> reported the observation of free-bound-bound spectra in their interpretation of recorded  $Mg_2$  spectra. In today's nomenclature, this process would be addressed as "photoassociation."

The absorption spectra of  $Mg_2$  vapor in a heated cell were already investigated by Balfour *et al.*<sup>12</sup> with the high spectral resolution of a 10.5 m grating spectrograph. They assigned a set of about 4000 absorption lines observed in the range from about 266 nm to about 388 nm, most of them for the main isotopologue  $^{24}Mg_2$ , but also about 300 lines of the isotopologue  $^{26}Mg_2$ , which they could observe by an enriched isotopic sample. From the assigned spectra, they derived Dunham parameters and Rydberg-Klein-Rees (RKR) potential energy curves (PEC), covering vibrational levels in the interval  $0 \leq v'' \leq 12$  for the ground state  $X^1\Sigma_g^+$ . Thanks to the storage of their lists of transition frequencies as the supplementary material at the journal, the data are still available, and we could use them beneficially for the interpretation of our spectra.

Stwalley<sup>13</sup> calculated the van der Waals interaction constant  $C_6$  from dipole polarizabilities of the Mg atom and determined an improved dissociation energy from the combination of the RKR potential<sup>12</sup> and  $C_6$ .<sup>14</sup> In a later effort, Li and Stwalley<sup>15</sup> evaluated photo plates taken by Balfour *et al.*<sup>12</sup> and assigned transitions of the (1–13) and (2–13) bands thus improving the modeling of the long-range part of the ground state and yielding a more reliable dissociation energy.

Scheingraber *et al.*<sup>11</sup> and Vidal *et al.*<sup>16</sup> analyzed fluorescence in  $Mg_2$  vapor induced by the UV-lines of an Ar<sup>+</sup> laser and dispersed by a 2 m grating spectrometer. They identified not only transitions from bound ground state levels to bound excited state levels and fluorescence back to bound ground state levels (bound-bound-bound), but also the above mentioned free-bound-bound spectra, and additionally bound-bound-free and free-bound-free spectra. They determined a

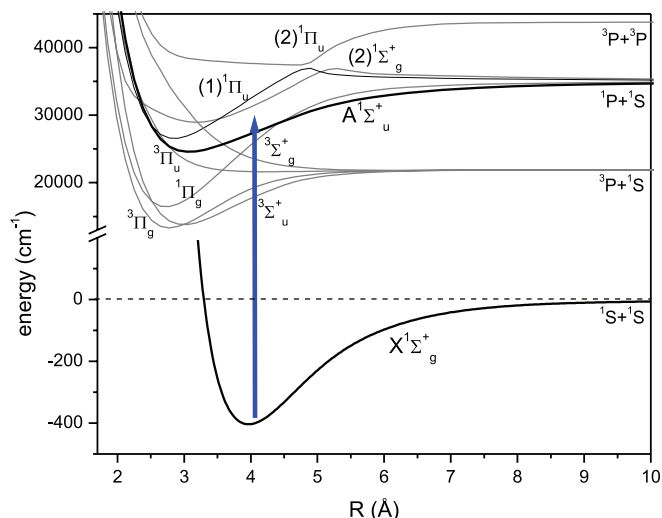


FIG. 1. The lowest electronic states of  $\text{Mg}_2$  according to *ab initio* calculations by Czuchaj *et al.*<sup>17</sup> Thick lines indicate potentials, which are important for the present work.

more precise ground state potential from their own data combined with those from Balfour *et al.*<sup>12</sup> employing their method of Inverted Perturbation Approach (IPA).<sup>16</sup> From their observation of structured fluorescence continua, they could characterize a section of the repulsive potential energy branch of the ground state above the dissociation limit.<sup>11</sup>

Several *ab initio* calculations of the electronic structure have been published. The most recent one by Czuchaj *et al.* derives PECs corresponding to dissociation asymptotes up to  $^3\text{P}+^3\text{P}$  (see Ref. 17 and references therein). Figure 1 gives an overview of the electronic structure of  $\text{Mg}_2$  based on that paper. Please notice the different scaling of the vertical axis. The ground state is only weakly bound by van der Waals forces and has much larger equilibrium internuclear distance compared to the excited states.

Tiesinga *et al.*<sup>18</sup> estimated the scattering length for cold collisions of Mg ground state atoms on the basis of the experimental results discussed above, of *ab initio* results from literature, of calculations of  $C_6$ ,  $C_8$ ,  $C_{10}$  long-range coefficients by Porsev *et al.*<sup>19</sup> and by their own *ab initio* calculations.

The present paper reports on a set of new spectroscopic investigations of the  $A^1\Sigma_u^+ - X^1\Sigma_g^+$  spectrum of  $\text{Mg}_2$ . It is motivated by the requirement of a more precise potential energy curve for the ground state and the desire of comparing more deeply empirical PECs determined by incorporating several distinct numerical model representations. The spectra were obtained by various experimental methods, which are described in the chapter “Experimental methods.” In section “Assignment...,” we develop the procedure of handling a dense absorption spectrum and obtaining as much information as possible for individual transition frequencies. Section “Analysis” comprises a description of the potential models and the fitting procedure, and we conclude with a discussion of the resulting potentials and the derived scattering lengths.

## II. EXPERIMENTAL METHODS

The  $\text{Mg}_2$  molecules are prepared in a heat pipe, which is similar to the ones used for our experiments on  $\text{Ca}_2$ <sup>5</sup> and

$\text{Sr}_2$ .<sup>6</sup> Therefore, a brief description should suffice here. About 10 g of Mg metal was placed into the center of a stainless steel tube, whose interior surface had been faced with a double layer of a stainless steel mesh. The heat pipe was prepared by baking it out under vacuum for several hours at about 700 K. Typical operation conditions were 40 to 80 hPa of Ar buffer gas and about 1100 K for the temperature of the central part of the heat pipe. We have checked spectra under various pressure conditions for pressure shifts. No such shifts were observed within the measurement precision. Thus, no corrections were applied. Typically, the heat pipe could be operated with stable optical throughput for about two hours. Then gradually crystals of Mg started growing from the tube wall into the optical path at both ends of the heated zone. In such cases, the oven was moved as close as possible to either end of the tube and the crystals were melted down into the mesh, and another two hours of operation were possible. After few such cycles of operation, an additional sample of Mg metal was put into the center to maintain the strength of the signals.

As the considered spectrum is in the UV between about 400 nm and 260 nm,<sup>12</sup> where we had no tunable laser available at that time, we started with classical absorption spectroscopy. The light of a broad band light source, a combination of a deuterium lamp, and a halogen lamp (DH2000, Ocean Optics Corp.) was collimated by a quartz lens through the heat pipe and imaged by another quartz lens onto the input diaphragm of our Fourier transform spectrometer (FTS) (FTS120HR, Bruker Optics Corp.). The spectral bandwidth was limited by a UV bandpass filter (UG11, Schott Corp.) to between 260 nm and 390 nm. The light was detected with a photomultiplier (R928, Hamamatsu Corp.). Under typical working conditions, a dense absorption spectrum between 26 000  $\text{cm}^{-1}$  and 33 000  $\text{cm}^{-1}$  was observed. In the region between 34 000  $\text{cm}^{-1}$  and 36 500  $\text{cm}^{-1}$ , essentially no light was transmitted through the heat pipe due to the strong absorption by the atomic resonance around 35 051  $\text{cm}^{-1}$ . Typically, the resolution of the FTS was set to 0.1  $\text{cm}^{-1}$ , which is of the same magnitude as the Doppler width (0.1  $\text{cm}^{-1}$  at the working temperature of the heat pipe for a transition frequency 30 000  $\text{cm}^{-1}$ ) and represents a reasonable compromise between resolution and measuring time. For the absorption spectrum, which was finally used for evaluation 300 interferograms were averaged and Fourier transformed. Figure 2 shows an example of the short interval from 28 120  $\text{cm}^{-1}$  to 28 150  $\text{cm}^{-1}$  of the recorded absorption spectrum. The black trace is the measured spectrum while the red dotted trace shows the simulated spectrum (more details of the simulation are given below) summing the most abundant isotopologues  $^{24}\text{Mg}_2$ ,  $^{24}\text{Mg}^{25}\text{Mg}$ , and  $^{24}\text{Mg}^{26}$  according to their natural abundance. The upper trace shows the difference between observed and simulated spectrum. The main peaks belong to the most abundant isotopologue, but many smaller features originate from overlap with the weaker isotopologues. Within Doppler resolution, there is probably no single, sufficiently isolated line.

For characterization of low-lying molecular states, it is more efficient to employ the method of laser-induced fluorescence (LIF) recorded under the high resolution of the FTS. We started such measurements with an UV-Ar+ laser

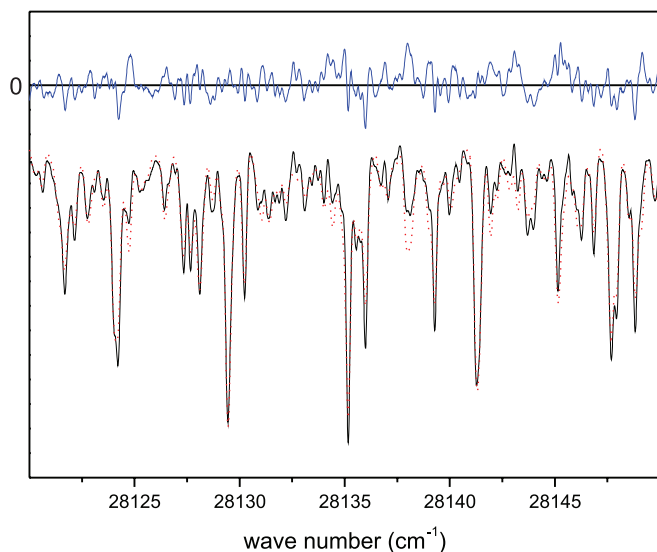


FIG. 2. Part of the recorded absorption spectrum (black, full line) together with the simulated spectrum (red, dotted) assuming constant electronic transition dipole moment and proper isotopic ratios of  $^{24}\text{Mg}_2$  (62%),  $^{24}\text{Mg}^{25}\text{Mg}$  (7.9%), and  $^{24}\text{Mg}^{26}\text{Mg}$  (8.7%), respectively. The upper (blue) trace shows the difference between measured and simulated spectra on the same signal scale.

(Spectra Physics model 2045) to which we had access for some time, essentially repeating the former experiment by Scheingraber *et al.*,<sup>11</sup> because their primary data are no longer available. The laser beam was guided through the hole of a pierced mirror through the center of the heat pipe. The laser-induced fluorescence counter propagating to the incoming laser beam was collected by the pierced mirror and directed through an imaging quartz optics onto the input diaphragm of the Fourier spectrometer. A filter UG11 limited the bandwidth, and the photomultiplier was used as the detector. With this configuration, we were able to record fluorescence progressions using the Ar+ laser with all lines UV mirrors installed and yielding up to 2 W of multiline UV output for the Ar+ lines 363 nm, 351 nm, and 334 nm. Later, a tunable TiSa laser (Technoscan) with a frequency doubler (SHG 110, Toptica Corp.) was employed for LIF experiments, using the same setup as for the Ar+ laser. However, here excitations to selected upper levels using the tunability of the TiSa laser were investigated. Figure 3 gives an example, their details will be discussed below in Sec. III.

### III. ASSIGNMENT AND TRANSITION FREQUENCIES

The isotopic abundance of natural Mg ( $^{24}\text{Mg}$  about 79%,  $^{25}\text{Mg}$  about 10%,  $^{26}\text{Mg}$  about 11%) yields a mixture of six isotopologues in the molecular gas with abundances of 62%, 7.9%, 8.7%, 1.1%, 1.0%, and 1.2% for  $^{24}\text{Mg}_2$ ,  $^{24}\text{Mg}^{25}\text{Mg}$ ,  $^{24}\text{Mg}^{26}\text{Mg}$ ,  $^{25}\text{Mg}^{26}\text{Mg}$ ,  $^{25}\text{Mg}_2$ , and  $^{26}\text{Mg}_2$ , respectively. The small vibrational frequency and the large equilibrium internuclear distance in the ground state as well as the high temperature of 1100 K yield a significant thermal population for all rovibrational levels of the ground state, so that the absorption spectrum shows a high density of lines and a substantial degree of blending of lines. In practice, this means that essentially no observed spectral feature is due to a single transition,

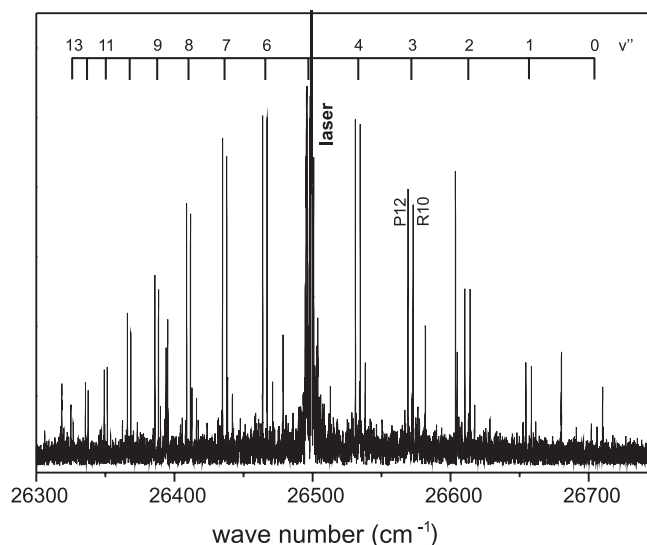


FIG. 3. Example of a fluorescence progression with P(12)/R(10) doublets, where R(10) (3–5) of  $^{24}\text{Mg}_2$  was excited at  $26499.328\text{ cm}^{-1}$  derived by a frequency doubled TiSa laser.

which presents a limitation regarding the accuracy of transition frequencies that can be derived from the obtained spectra.

To overcome this limitation at least partly, we set up a program, which simulates the spectrum in a specified frequency interval. It uses PECs, the best ones known at the actual stage of evaluation, for the lower and the upper states and determines the transition frequencies from differences of energy eigenvalues of these PECs, while intensities are calculated according to the Franck-Condon principle assuming a constant electronic transition dipole moment. Such calculations are done for the three most abundant isotopologues (which is adequate due to the signal-to-noise ratio of our spectra in relation to the intensities of the least abundant isotopologues) and the spectra are generated by calculating line shapes of proper width for any such transition and adding them up for simulation of the experimental spectrum. Starting with IPA potentials from Ref. 16 and improving the PECs iteratively by adding new data, quantum numbers were assigned to the lines in the spectra. Transition frequencies were then determined from the experimental spectra by fitting the positions of simulated lines located in a certain chosen frequency interval to the experimental spectrum in that interval while leaving the calculated intensities fixed. As the positions of weak lines are not well determined in most cases, only the frequencies of the most prominent lines were accepted for the final data set. For strong lines with not too much overlap from other structures an uncertainty of  $0.01\text{ cm}^{-1}$  was assumed, for more severely blended structures the uncertainty was estimated from accounting for the influence of the considered line on the observed structure. Typical values range from  $0.015\text{ cm}^{-1}$  to  $0.05\text{ cm}^{-1}$ . This leads to about a factor of 3 improvement of the precision compared to the earlier measurements by Balfour *et al.*<sup>12</sup> By this treatment, the major part of the set of transition frequencies listed by Balfour *et al.*<sup>12</sup> for  $^{24}\text{Mg}_2$  have been replaced by new and more accurate ones.

With the frequency doubled TiSa laser, we excited levels, which most favorably give fluorescence to as many ground

state levels as possible expected from the Franck-Condon principle and yield the largest Franck-Condon factors for transitions to the highest vibrational levels of the ground state. For the  $\text{Mg}_2$  A-X system, the Franck-Condon factors (FCF) depend strongly on rotation, essentially any rovibrational band involves only a limited span of 20 to 30 rotational lines with reasonable intensities. Calculation of FCF reveals that the upper state vibrational levels  $v' = 2$  and  $v' = 3$  promise the largest FCF for fluorescence to the higher vibrational levels of the ground state. Exciting the  $(v' - v'') = (3 - 5)$  band around  $26\,500\text{ cm}^{-1}$ , we recorded systematically fluorescence progressions due to the excitation of various selected rotational lines. Figure 3 shows the fluorescence progression when exciting the R(10) line of the (3–5) band of  $^{24}\text{Mg}_2$ . R- and P-lines to vibrational levels  $0 \leq v'' \leq 13$  can be easily identified. Also, additional lines due to collisional relaxation show up. However, lines to levels  $v'' \geq 14$  are not visible within the present signal-to-noise ratio, despite the fact that the FCF for the transition to  $v'' = 0$  is smaller than that for  $v'' = 14$  and  $v'' = 15$ . The reason for this is not yet clear, it might show the limitation of the FC principle due to variation of the transition dipole moment with R. Here, *ab initio* calculations could guide the analysis.

The spectra of the LIF measurements were treated similar to the absorption spectrum, but with the advantage that there were typically no overlapping structures. The frequencies of the progression lines were introduced as frequency differences referred to one selected line in the progression, in order to restrict their information content to the ground state alone and by this to reduce the correlation between the parameters of lower and upper states and the influence of Doppler shift due to possible detuning of the exciting laser with respect to the center of the molecular transition.

An overview of the range of quantum numbers of the levels involved in the characterization of the  $X^1\Sigma_g^+$  ground state of  $\text{Mg}_2$  is given in Figure 4. The diagram reveals that  $v'' = 13$  is the highest vibrational level observed. Rotational

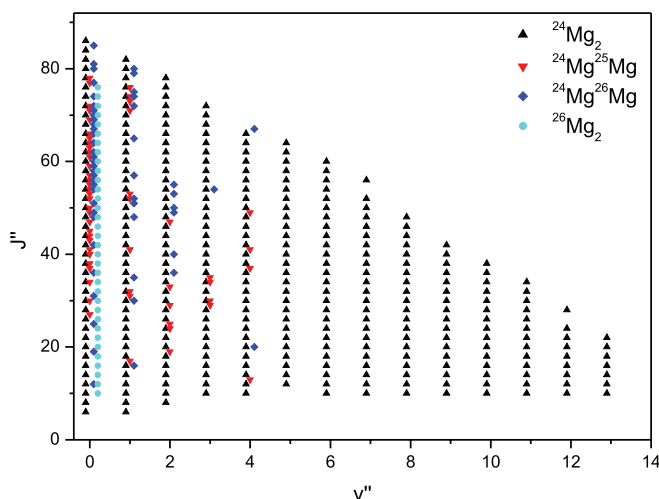


FIG. 4. Range of vibrational quantum numbers  $v''$  and rotational quantum numbers  $J''$  of the energy levels used for the characterization of the  $X^1\Sigma_g^+$  ground state of  $\text{Mg}_2$  in the present study. The data on  $^{26}\text{Mg}_2$  were taken from Ref. 12.

quantum numbers in the ground state are limited to  $J'' \leq 86$  for  $v'' = 0$  and less for  $v'' > 0$ , bound levels with higher rotational quantum numbers do not exist in the ground state because of rotational dissociation. Levels very close to the dissociation limit are shifted and broadened by tunneling through the rotational barrier. Altogether 334 levels of  $^{24}\text{Mg}_2$ , 55 levels of  $^{24}\text{Mg}^{25}\text{Mg}$ , 51 levels of  $^{24}\text{Mg}^{26}\text{Mg}$ , and 34 levels of  $^{26}\text{Mg}_2$  are available for the determination of the ground state PEC, stemming from altogether about 4952 transition frequencies for  $v' \leq 28$  of  $A^1\Sigma_u^+$  in the range between  $26\,000\text{ cm}^{-1}$  and  $31\,200\text{ cm}^{-1}$ , or from frequency differences by means of the fluorescence progressions. The range of vibrational quantum numbers for the upper state has been limited in order to exclude regions in the upper state, where perturbations have been identified. Few narrow frequency intervals of the absorption spectrum were discarded due to emission lines in the lamp spectrum.

#### IV. ANALYSIS

The experimental data are used for direct fits of PECs. By far, most of the data are transition frequencies, which involve energy levels of two electronic states, so the approach of choice is to fit two PECs simultaneously. Calculated energies are determined as eigenvalues of the radial Schrödinger equation in the internuclear distance  $R$  for each electronic state with an effective Hamiltonian of the form (see, e.g., Ref. 21) appropriate for electronic states with symmetry  $^1\Sigma$ :

$$\mathbf{H}_{\text{eff}} = -\frac{\hbar^2}{2\mu} \frac{\partial^2}{\partial R^2} + U(R) + U_{\text{corr}}(R) + \frac{\hbar^2 \cdot [1 + \alpha(R)] \cdot J(J+1)}{2\mu R^2}, \quad (1)$$

where  $\mu$  is the reduced mass and  $\hbar$  is Planck's constant.  $U(R)$  is the Born-Oppenheimer potential and  $U_{\text{corr}}$  and  $\alpha$  are the adiabatic and non-adiabatic Born-Oppenheimer corrections (BOC), respectively, which account for small deviations from the Born-Oppenheimer approximation by coupling to different electronic states, which could become obvious if more than one isotopologue or high rotational quantum numbers are involved. For details, the reader is referred to the paper cited above. The adiabatic correction  $U_{\text{corr}}(R)$  is mass dependent and can only be distinguished from  $U(R)$  if data of different isotopic species of the molecule are available. It was taken into account, but only for the upper state, as was already mentioned by Vidal *et al.*<sup>16</sup> The non-adiabatic BOC was not significant in the present evaluation.

During the fit, the eigenvalues for the lower and the upper levels are calculated for each optical transition with the respective potentials including possible shifts by tunnel effect due to the rotational barrier. The difference of the calculated transition frequency to the measured one is used in a weighted least squares fit in which the various representations of the PECs are adjusted, respectively, to yield a minimum  $\chi^2$

$$\chi^2 = \sum_j \left( \frac{\text{obs}_j - \text{cal}_j}{\Delta \text{obs}_j} \right)^2, \quad (2)$$

where  $\text{obs}_j$  are the observed transition frequencies,  $\text{cal}_j$  the calculated values, and  $\Delta\text{obs}_j$  the estimated uncertainties of the experimental values. For the fitting of such nonlinear problems, we use the MINUIT program package.<sup>22</sup> Sections IV A–IV E describe four different kinds of numerical representations of the PECs.

### A. X-representation of potential energy curves

In the so-called X-representation, a PEC  $U_X(R)$  (see, e.g., Ref. 8) is cut into three parts. The central well around the potential minimum, labeled by CP, with  $R_i \leq R \leq R_o$  is represented as a finite power series

$$U_X^{\text{CP}}(R) = \sum_{i=1}^n a_i \xi(R)^i \quad (3)$$

with a nonlinear variable function  $\xi$  of internuclear separation  $R$ :

$$\xi(R) = \frac{R - R_m}{R + b R_m}. \quad (4)$$

The  $\{a_i\}$  are adjustable parameters. The parameter  $b$  determines the pole at small  $R < R_i$ , and allows to some degree to account for the steep repulsive branch, and  $R_m$  is the expansion center, chosen typically close to the equilibrium internuclear distance  $R_e$ . Those two parameters are found once by initially modeling a preliminary RKR potential with the analytic form (3) and kept fixed in subsequent fits of the parameters  $a_i$ . The position of energy zero is selected at  $R = R_m$ .

The potential can be continuously and differentially extrapolated for  $R < R_i$  with

$$U_X^{\text{SR}}(R) = B e^{-C(R-R_i)} \quad (5)$$

by adjusting the parameters  $B$  and  $C$  accordingly at  $R_i$ .

For large internuclear distances  $R > R_o$ , the standard long-range form of molecular potentials is adopted

$$U_X^{\text{LR}}(R) = D_m - \sum_i C_i / R^i. \quad (6)$$

For the  $X^1\Sigma_g^+$  of  $\text{Mg}_2$ , terms with  $i = 6, 8, 10$  were used, taking the  $C_i$  from literature.  $C_{12}$  and  $D_m$  are adjusted for a continuous and differentiable transition at  $R_o$ .

### B. Le Roy's MLR representation

The analytic representation of PECs defined above is rather flexible and has been employed in many examples. However, it bears some intrinsic arbitrariness by the requirement of a reasonable choice of  $R_i$  and  $R_o$ . The choice of  $R_i$  is usually not very critical selecting a value sufficiently shorter than the expected inner turning points, compare initial RKR curves. However, the detailed choice of  $R_o$  will influence the dissociation energy, even if, as usual done,  $R_o$  is chosen to be close to or larger than the Le Roy radius<sup>23</sup> (7.2 Å for the  $X^1\Sigma_g^+$  state of  $\text{Mg}_2$ <sup>24</sup>) and reliable dispersion coefficients  $C_i$  are known.

There are other potential representations, such as, e.g., the ‘‘Morse Long Range’’ (MLR) form developed by Le Roy

(see Ref. 25 and references therein), which have built in the form of a bound state and are also flexible but avoid transitions between different mathematical representations at connection points, such as  $R_i$  or  $R_o$  above. They describe the PEC by a single function over the full range of relevant internuclear distances. This approach was employed here as well for the representation of the ground state potential. For details, we refer the reader to the original paper<sup>25</sup> and the discussions therein. Here, we will give only the main formulas for easier understanding and defining the fit parameters.

The PEC is represented in the form

$$U_{MLR}(R) = D_e \left[ 1 - \frac{u_{LR}(R)}{u_{LR}(R_e)} \exp\left[-\beta_p^q(R) \cdot y_p^{eq}(R)\right] \right]^2 \quad (7)$$

with  $D_e$  being the well depth, respectively, the dissociation energy, and  $R_e$  the equilibrium internuclear distance or the position of the potential minimum. The radial variable  $y_p(R)$  is defined by the superscript *ref* with respect to some chosen reference internuclear distance  $R_{ref}$  as

$$y_p^{ref}(R) = \frac{R^p - R_{ref}^p}{R^p + R_{ref}^p}. \quad (8)$$

The subscript  $p$  at  $y$  refers to the chosen power  $p$  and a superscript *eq* instead of *ref* to the equilibrium internuclear distance  $R_e$ . The coefficient  $\beta_p^q(R)$  in (7) is defined as

$$\beta_p^q(R) = y_p^{ref}(R) \beta_\infty + [1 - y_p^{ref}(R)] \sum_{i=0}^N \beta_i [y_p^{ref}(R)]^i, \quad (9)$$

which forces the required long-range behavior for  $R \rightarrow \infty$

$$U^{MLR}(R) = D_e - u_{LR}(R) + \dots \quad (10)$$

with

$$u_{LR}(R) = \sum_i \frac{C_i}{R^i}, \quad (11)$$

if the asymptotic behavior of  $\beta$  is such that

$$\lim_{R \rightarrow \infty} \beta(R) = \beta_\infty = \ln[2D_e/u_{LR}(R_e)]. \quad (12)$$

The  $C_i$  are the contributions of the van der Waals long-range interactions between the two atoms and  $p$  should be larger than the difference of the exponents between the highest to lowest order in the long-range function of Eq. (11). Then the expansion of Eq. (7) in powers of  $1/R$  leads only to contributions with an exponent greater than the highest order used in Eq. (11). In the present example of  $\text{Mg}_2$ , we set  $p = 5$  because we want to consider long-range parameters from  $C_6$  to  $C_{10}$ .  $R_{ref}$  is typically chosen larger than  $R_e$  and  $q$  is set normally smaller than  $p$ , so that the function in Eq. (8) will not become too steep for increasing  $i$ .

The basic functional form in this approach is a Morse potential, which already has the shape of a bound potential needing essentially only two parameters in the exponent. In the MLR approach, the simple exponent has been replaced by a more flexible series ansatz, and desired long-range behavior is built in.

### C. Modified Tang-Toennies representation

The ground states  $X^1\Sigma_g^+$  of diatomic alkaline earth metal molecules are generally weakly bound, the bond being essentially due to van der Waals forces. For such PECs, Tang and Toennies (TT)<sup>26–28</sup> proposed a simple functional representation

$$U_{TT}(R) = A e^{-bR} - \sum_{n=3}^{\infty} \left[ 1 - \left( \sum_{k=0}^{2n} \frac{(bR)^k}{k!} \right) e^{-bR} \right] \frac{C_{2n}}{R^{2n}} + T_{dis}, \quad (13)$$

where we have added  $T_{dis}$ , which is chosen such that the potential minimum has energy zero. The first term on the right side represents the repulsive and the second term the attractive damped dispersive part.  $A$  and  $b$  are effective parameters of the repulsive potential,<sup>28</sup> while the  $C_{2n}$  are the dispersion coefficients. In practice, the infinite sum in Eq. (13) is truncated to some  $n_{max}$ , which is the index of the van der Waals coefficient of highest order used. Choosing  $n_{max} = 5$ , as is often done, the TT potential is determined by only 5 parameters for the whole potential from small to large internuclear distances.

For the estimation of higher order van der Waals coefficients, TT proposed a semi-empirical recursion formula

$$C_{2n+4} = \left( \frac{C_{2n+2}}{C_{2n}} \right)^3 C_{2n-2}. \quad (14)$$

One attractive aspect of the TT potential is, that in its reduced form,<sup>28</sup> it allows by simple combining rules<sup>29</sup> predictions of unknown potentials of the same kind of molecules. This was shown by TT on examples of mixed rare-gas systems and by Sheng *et al.*<sup>30</sup> on examples of mercury rare-gas systems.

Recently, a set of papers appeared showing that the experimentally determined ground state PECs of the alkaline earth metal dimers  $\text{Ca}_2$ ,<sup>31</sup>  $\text{Sr}_2$ ,<sup>32</sup> and  $\text{Mg}_2$ <sup>33</sup> can be approximated with the Tang-Toennies representation according Eq. (13). The parameters  $A$  and  $b$  were derived from experimental values of the dissociation energy and the equilibrium internuclear distance  $R_e$ , while the dispersion coefficients were taken from most recent theoretical calculations. However, in all cases the comparison was done with PECs of other representations derived from experiments and not by comparing eigen values of rovibrational states. We did this and found deviations in the order of  $10 \text{ cm}^{-1}$  and more, which is unacceptable for spectroscopic standards. We will include the Tang-Toennies representation into a direct fit of PECs to experimental data. Such approach will give much more weight for statements on the power of this model.

However, doing this for the ground state PEC of  $\text{Mg}_2$  with the new precise data available now, it immediately turned out, that a single parameter  $b$  would not be sufficient to account for the precision of the experimental data, and also an addition of further dispersion parameters up to  $n = 9$  did not help.

So, we introduced an expansion for  $b$  as a function of the internuclear distance  $R$ , with extension parameters such as Eqs. (4) or (8) to gain more flexibility. This is an empirical approach still with the goal to use as few adjustable parameters as possible for a description of the observations within their experimental uncertainties and to keep the benefits of the general form of TT-potentials,

$$b(R) = b_0 + \frac{R_c}{R + R_c} \sum_{i=1}^m b_i \left( \frac{R - R_m}{R + R_m} \right)^i. \quad (15)$$

The factor  $R_c/(R + R_c)$  in front of the sum damps the polynomial to avoid unphysical steep increase for large  $R$ , and  $R_c$  is the cut-off radius beyond which the damping starts acting. It was set to  $40 \text{ \AA}$  in all fits and thus it is far outside the region supported by experimental data. We will not consider the physical meaning of the additional parameters  $b_i$ .

### D. Analytic representation by Chebychev polynomials

Recently, Busevica *et al.*<sup>34</sup> demonstrated the flexibility of a PEC representation based on a Chebychev expansion of the form

$$U_{CPE}(R) = T_{dis} - \frac{\sum_{k=0}^m c_k T_k(y_p)}{1 + (R/R_{ref})^n}, \quad (16)$$

where  $T_k(y)$  are the Chebychev polynomials of first kind and  $y_p \in [-1, 1]$  is the reduced radial variable similar to that in Eq. (8)

$$y_p(R; R_{min}, R_{ref}) = \frac{R^p - R_{ref}^p}{R^p + R_{ref}^p - 2R_{min}}. \quad (17)$$

Here,  $p \in [1, 2, \dots]$  is a small positive integer and  $R_{ref} > R_{min} > 0$  is the center of power expansion. This model covers the whole range between some chosen  $R_{min}$  and infinity without any need of transition points and has built in the long-range behavior of the lowest order of the van der Waals interaction by  $n$ . Compared to other polynomials or the simple power expansion in Sec. IV A, the Chebychev polynomials offer better convergence properties due to the fact that they form a complete and orthogonal basis set, leading to mainly monotonous decrease of the magnitude of the expansion coefficients  $c_k$ . The long-range behavior can be written as<sup>34</sup>

$$U_{CPE}(R) = T_{dis} - \frac{C_n}{R^n} - \frac{C_{n+p}}{R^{n+p}} + \dots, \quad (18)$$

where

$$C_n = R_{ref}^n \sum_{k=0}^m c_k, \quad (19)$$

$$C_{n+p} = 2(R_{min}^p - R_{ref}^p) R_{ref} \sum_{k=0}^m c_k k^2. \quad (20)$$

In this representation, the long-range parameters could result from the fit of the inner part of the potential defined by the experimental data. However, we will here introduce constraints in the fit for obtaining a solution with  $C_6$  and  $C_8$  close to their *ab initio* values, setting  $n = 6$  and  $p = 2$ .  $T_{dis}$  is chosen for energy zero at the potential minimum.

## E. Results

For the fits, only upper state levels with vibrational quantum numbers  $v' \leq 28$  were used, which are almost free from perturbations. In general, for an optimum fit result, the parameters of both upper and lower state PECs have to be varied. However, as a comparison of various representations of PECs for the ground state was aimed at, exactly the same values of parameters for the upper state was used in all final fits. These parameters were taken from the best fit with X-representations for both upper and lower state. We will defer a detailed discussion of the upper state  $A^1\Sigma_u^+$  to a future publication, because the evaluation of the spectra with an extended set of vibrational levels including perturbations in higher  $v'$  levels by the state  $^1\Pi_u$  and possibly predissociation by  $^3\Pi_u$  (see Fig. 1) is still under way.

In the final stage of the fits, we carefully inspected the data for the influence of tunnel effect due to the rotational barrier for high  $J''$ , and removed transitions listed in the older data set, which were obviously wrongly assigned, such as transitions comprising levels  $(v'', J'') = (0, 90), (0, 88), (1, 84)$ . Those are either not supported by the present potentials or are broadened and shifted by tunnel effect and could not be identified in the new measurements.

The uppermost level of the ground state observed by LIF, namely  $v'' = 13, J'' = 22$ , corresponds to an energy calculated with the X-representation to be  $428.372 \text{ cm}^{-1}$ . No higher levels could be found, despite the fact that the Franck-Condon factor from the same excited level is smaller only by about a factor of two comparing, e.g., the  $P(22)(3-13)$  transition with  $P(22)(3-14)$  or with  $P(22)(3-0)$ , which has been seen but whose FCF is half as large. This is not yet understood, an explanation could be a significant variation on R of the transition moment, which is assumed constant by applying the Franck-Condon principle. To our knowledge, yet no *ab initio* calculations of transition dipole moments of  $\text{Mg}_2$  do exist, so at present this assumption remains a hypothesis.

The results of the four fits with the X-, the MLR-, the modified Tang-Toennies-, and the Chebychev-representation for the ground state are collected in Tables I–IV, respectively.

As already mentioned, an adiabatic BOC has been taken into account for the state  $A^1\Sigma_u^+$  in addition to the normal mass effect for the vibration and rotation for fitting all observed isotopologues simultaneously, because the change in reduced mass is fairly large for such light atoms, such as Mg. This was not necessary for the shallow potential of state  $X^1\Sigma_g^+$ , thus these four solutions of the potential curve are independent of the reduced mass at least within the present experimental uncertainty limit, on average  $0.02 \text{ cm}^{-1}$  for calculated rovibrational eigen values.

## V. DISCUSSION AND CONCLUSION

The reduced standard deviations  $\sigma = \chi_{\min}/\sqrt{(N_{\text{obs}} - N_p)}$ ,  $N_{\text{obs}}$  being the number of observations and  $N_p$  the number of free fit parameters, of the various fits are very close to each other and essentially 1.05 in all cases, the standard deviations of the fits are  $0.022 \text{ cm}^{-1}$ . The fit quality given by the obtained reduced standard deviations

TABLE I. Parameters for the potential curve of the ground state  $X^1\Sigma_g^+$  of  $\text{Mg}_2$  for the X-representation. See text for details of the short-range representation.

Parameter	Value
$R < R_i = 3.27 \text{ \AA}$	
B ( $\text{cm}^{-1}$ )	$0.40399294 \times 10^3$
C ( $\text{\AA}^{-1}$ )	$-0.15132844 \times 10^2$
$R_i \leq R \leq R_o = 8.5 \text{ \AA}$	
$R_m$ ( $\text{\AA}$ )	3.890 390
b	0.0
$a_1$ ( $\text{cm}^{-1}$ )	$-0.770 548 964 164 001 222 \times 10^{-2}$
$a_2$ ( $\text{cm}^{-1}$ )	$0.705 289 125 191 954 554 \times 10^4$
$a_3$ ( $\text{cm}^{-1}$ )	$-0.179 327 568 767 261 764 \times 10^5$
$a_4$ ( $\text{cm}^{-1}$ )	$0.228 278 059 421 389 626 \times 10^5$
$a_5$ ( $\text{cm}^{-1}$ )	$-0.144 881 409 083 685 430 \times 10^5$
$a_6$ ( $\text{cm}^{-1}$ )	$-0.638 841 357 804 591 826 \times 10^5$
$a_7$ ( $\text{cm}^{-1}$ )	$0.201 722 011 755 478 365 \times 10^6$
$a_8$ ( $\text{cm}^{-1}$ )	$-0.286 947 115 902 508 434 \times 10^6$
$a_9$ ( $\text{cm}^{-1}$ )	$0.528 096 212 291 666 190 \times 10^6$
$a_{10}$ ( $\text{cm}^{-1}$ )	$-0.841 629 359 994 647 559 \times 10^6$
$a_{11}$ ( $\text{cm}^{-1}$ )	$0.510 277 917 592 615 297 \times 10^6$
$R_o < R$	
$C_6$ ( $\text{cm}^{-1}\text{\AA}^6$ )	$0.302 17 \times 10^7$ (Refs. 19 and 20)
$C_8$ ( $\text{cm}^{-1}\text{\AA}^8$ )	$0.560 07 \times 10^8$ (Ref. 20)
$C_{10}$ ( $\text{cm}^{-1}\text{\AA}^{10}$ )	$0.104 19 \times 10^{10}$ (Ref. 20)
$C_{12}$ ( $\text{cm}^{-1}\text{\AA}^{12}$ )	$0.344 618 98 \times 10^{11}$ <sup>a</sup>
$D_m$ ( $\text{cm}^{-1}$ )	430.472 <sup>a</sup>
Std. dev. of fit ( $\text{cm}^{-1}$ )	0.022
Red. std. dev. $\sigma$	1.048
Derived constants	
$R_e$ ( $\text{\AA}$ )	3.890 39
$D_e$ ( $\text{cm}^{-1}$ )	430.472

<sup>a</sup>Adjusted for continuously differentiable transition at  $R_o$ .

TABLE II. Parameters for the potential curve of the ground state  $X^1\Sigma_g^+$  of  $\text{Mg}_2$  for the MLR representation.

Parameter	Value
$D_e$ ( $\text{cm}^{-1}$ )	430.369
$R_e$ ( $\text{\AA}$ )	3.890 39
$R_{\text{ref}}$ ( $\text{\AA}$ )	4.0
$p$	5
$q$	3
$\beta_0$	$-0.166 551 033 592 512 887 \times 10^1$
$\beta_1$	$-0.294 159 018 281 270 335 \times 10^{-1}$
$\beta_2$	$-0.104 633 090 905 496 307 \times 10^1$
$\beta_3$	$-0.324 453 179 411 172 965$
$\beta_4$	$-0.184 420 236 755 870 848 \times 10^1$
$\beta_5$	$0.114 228 141 585 836 918 \times 10^1$
$\beta_6$	$0.119 434 493 806 085 307 \times 10^1$
$\beta_7$	$-0.773 024 102 172 378 935 \times 10^1$
$\beta_8$	$0.753 234 036 484 323 610 \times 10^1$
$\beta_\infty$	$-0.132 885 338 652 134 144 \times 10^1$
$C_6$ ( $\text{cm}^{-1}\text{\AA}^6$ )	$0.302 17 \times 10^7$ (Refs. 19 and 20)
$C_8$ ( $\text{cm}^{-1}\text{\AA}^8$ )	$0.560 07 \times 10^8$ (Ref. 20)
$C_{10}$ ( $\text{cm}^{-1}\text{\AA}^{10}$ )	$0.104 19 \times 10^{10}$ (Ref. 20)
Std. dev. of fit ( $\text{cm}^{-1}$ )	0.022
Red. std. dev. $\sigma$	1.049

TABLE III. Parameters for the potential curve of the ground state  $X^1\Sigma_g^+$  of  $Mg_2$  for the modified Tang-Toennies representation.

Parameter	Value
$T_{dis}$ ( $\text{cm}^{-1}$ )	430.144
$R_m$ ( $\text{\AA}$ )	3.889 263 02
$A$ ( $\text{cm}^{-1}$ )	$0.108\,595\,626\,126\,240\,799 \times 10^7$
$b_0$ ( $\text{\AA}^{-1}$ )	$0.101\,294\,170\,235\,559\,422 \times 10^1$
$b_1$ ( $\text{\AA}^{-1}$ )	$0.773\,713\,623\,088\,733\,982 \times 10^{-1}$
$b_2$ ( $\text{\AA}^{-1}$ )	0.240 474 251 400 950 606
$b_3$ ( $\text{\AA}^{-1}$ )	$0.485\,416\,213\,402\,752\,739 \times 10^1$
$b_4$ ( $\text{\AA}^{-1}$ )	$-0.269\,718\,630\,992\,724\,329 \times 10^1$
$b_5$ ( $\text{\AA}^{-1}$ )	$-0.345\,900\,032\,322\,231\,823 \times 10^2$
$b_6$ ( $\text{\AA}^{-1}$ )	$0.131\,975\,570\,704\,269\,131 \times 10^3$
$C_6$ ( $\text{cm}^{-1}\text{\AA}^6$ )	$0.302\,17 \times 10^7$ (Refs. 19 and 20)
$C_8$ ( $\text{cm}^{-1}\text{\AA}^8$ )	$0.560\,07 \times 10^8$ (Ref. 20)
$C_{10}$ ( $\text{cm}^{-1}\text{\AA}^{10}$ )	$0.104\,19 \times 10^{10}$ (Ref. 20)
Std. dev. of fit ( $\text{cm}^{-1}$ )	0.022
Red. std. dev. $\sigma$	1.049
Derived constants	
$R_e$ ( $\text{\AA}$ )	3.890 42
$D_e$ ( $\text{cm}^{-1}$ )	430.144

is practically the same in all cases, thus the fit results are equivalent in the statistical sense.

However, the number of fit parameters is different. While the simple X-representation needs 11 freely varied parameters and 4 fixed parameters, namely  $b$ ,  $R_m$ ,  $R_i$ , and  $R_o$ , the Chebychev-representation takes profit from its better convergence properties and the built-in long-range behavior, thus it needs only 10 freely varied parameters and 2 fixed ones ( $R_{min}$

TABLE IV. Parameters for the potential curve of the ground state  $X^1\Sigma_g^+$  of  $Mg_2$  for the Chebychev expansion model.

Parameter	Value
$T_{dis}$ ( $\text{cm}^{-1}$ )	429.946
$R_{min}$ ( $\text{\AA}$ )	2.700 00
$R_{ref}$ ( $\text{\AA}$ )	4.540 00
$p$	2
$n$	6
$c_1$ ( $\text{cm}^{-1}$ )	$0.115\,612\,010\,546\,087\,618 \times 10^3$
$c_2$ ( $\text{cm}^{-1}$ )	$-0.104\,934\,266\,127\,811\,452 \times 10^4$
$c_3$ ( $\text{cm}^{-1}$ )	$0.903\,443\,935\,869\,525\,717 \times 10^3$
$c_4$ ( $\text{cm}^{-1}$ )	$-0.388\,090\,871\,752\,716\,339 \times 10^3$
$c_5$ ( $\text{cm}^{-1}$ )	$0.920\,027\,087\,879\,408\,896 \times 10^2$
$c_6$ ( $\text{cm}^{-1}$ )	$-0.748\,779\,898\,698\,819\,224 \times 10^{-1}$
$c_7$ ( $\text{cm}^{-1}$ )	$-0.423\,404\,425\,675\,817\,464 \times 10^2$
$c_8$ ( $\text{cm}^{-1}$ )	$0.247\,172\,340\,168\,360\,236 \times 10^2$
$c_9$ ( $\text{cm}^{-1}$ )	$-0.595\,640\,136\,673\,318\,921 \times 10^1$
$c_{10}$ ( $\text{cm}^{-1}$ )	$0.484\,690\,380\,785\,059\,993 \times 10^1$
$C_6$ ( $\text{cm}^{-1}\text{\AA}^6$ )	$0.302\,262\,20 \times 10^7$ <sup>a</sup>
$C_8$ ( $\text{cm}^{-1}\text{\AA}^8$ )	$0.560\,079\,63 \times 10^8$ <sup>a</sup>
Std. dev. of fit ( $\text{cm}^{-1}$ )	0.022
Red. std. dev. $\sigma$	1.032
Derived constants	
$R_e$ ( $\text{\AA}$ )	3.890 40
$D_e$ ( $\text{cm}^{-1}$ )	429.946

<sup>a</sup>Calculated with Eqs.(19) or (20) and constraints in the fit to result close to the theoretical values by Refs. 19 and 20.

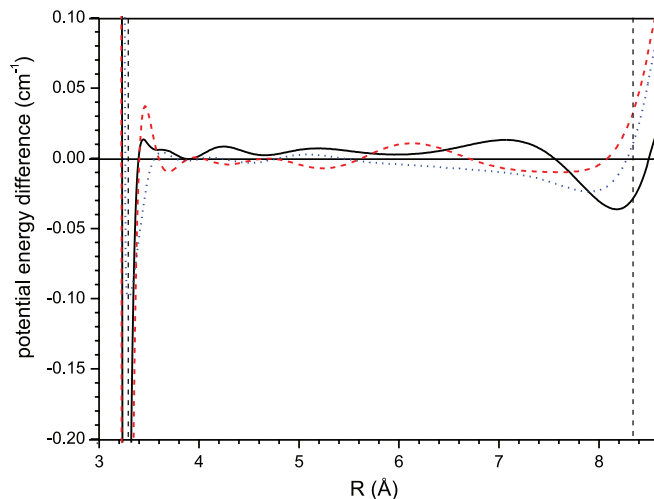


FIG. 5. Comparison of potential energy curves. Black, solid:  $U_X - U_{MLR}$ , red, dashed:  $U_X - U_{TT}$ , blue, dotted:  $U_X - U_{Cheb}$ . The range of internuclear distances covered by the data is indicated by the vertical dashed lines.

and  $R_{ref}$ ) for the whole range of internuclear distances. Models already naturally providing by their construction a shape corresponding to a bound potential, such as MLR and TT, are hoped to require even fewer numbers of parameters (actually, 11 and one fixed ( $R_{ref}$ ) for MLR and 9 for TT) and would give the most compact representation for this example of a not very deep potential. Only the TT-representation shows the expected advantage. We should note, that we cannot conclude from our effort that we always arrived at the lowest possible number of parameters needed in the cases studied.

The standard deviations reveal an improvement of more than a factor of 3 compared to previous experimental precision ( $\approx 0.07 \text{ cm}^{-1}$  <sup>16</sup>). It is still limited by the large Doppler width of the light molecule  $Mg_2$  at such elevated temperatures (1100 K) and by the severe overlap of many lines in the absorption spectrum because of the dense levels structure and the isotopic composition. The reliability of the well depth was improved compared to previous results, due to the inclusion of tunnel effect for levels close to the asymptote and removed wrongly assigned levels.

Differences of the resulting PECs from the four approaches are drawn in Figure 5 by comparing the X-representation with the three others in the bound region of internuclear distance. The PECs are supported by discrete spectral data from 3.27  $\text{\AA}$  to 8.33  $\text{\AA}$ . There are differences of up to  $\pm 0.25 \text{ cm}^{-1}$  in the short-range region, overshooting the drawing. For the long-range region, similar differences in absolute values appear due to different extrapolations of the models to the dissociation energy. While the X, MLR, and TT models are constructed with fixed long-range coefficients, for the Chebychev model only  $C_6$  and  $C_8$  were calculated from Eqs. (19) and (20), respectively, and the fit was forced by additional constraints to adjust  $C_6$  and  $C_8$  closely to the theoretical values, which were incorporated in the other approaches. Therefore, the long-range part and the dissociation energy of the Chebychev model might be not as reliable as that of the other models.

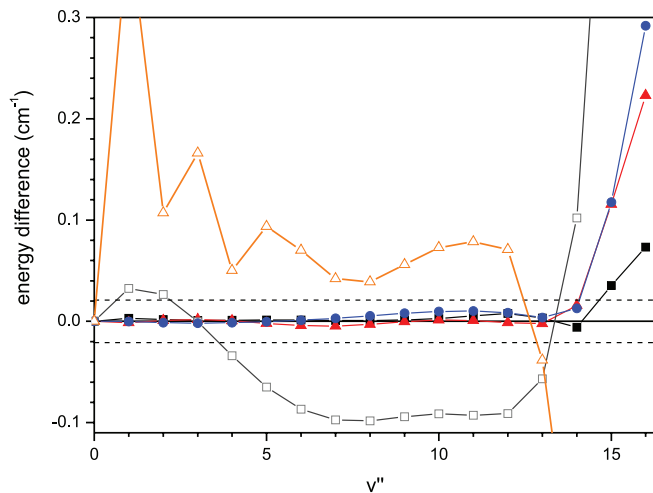


FIG. 6. Comparison of level energy differences  $v'', J'' = 0$  with respect to the X-representation calculated from the various potential models (MLR: full squares, TT: full triangles, Chebychev: full circles), for details see text. The differences with term energies from Ref. 16 (open squares) are calculated with the Dunham parameters of their Table IV, and differences with level energies from Ref. 18 (open triangles) are calculated using the spline interpolated IPA potential of their Table II. Lines connecting the points are only drawn for guiding the eye.

While the differences of the potentials in Figure 5 appear to be quite large in some regions compared to the experimental uncertainty ( $0.02 \text{ cm}^{-1}$ ), the differences of eigenvalues in these potentials are much smaller. This originates from integration over an extended R-interval when determining the eigenvalues. Figure 6 shows the energy differences of the level energies  $v'', J'' = 0$  for the potential representations MLR, TT, or Chebychev with the X-representation as reference, all referred to their level  $v'' = 0, J'' = 0$ . These differences are very well within the interval given by the standard deviations of the fits, indicated by the dashed horizontal line, for the levels  $1 \leq v'' \leq 13$  supported by data. The deviations increase for levels extrapolated closer to the asymptote, which is about  $20 \text{ cm}^{-1}$  above the level  $v'' = 13, J'' = 0$ . For comparison, the differences of term energies calculated with the eigenvalues  $v'', J'' = 0$  of the IPA-potential reported in Ref. 18 and with the Dunham parameters of Table IV of Ref. 16 are also shown in Fig. 6. Here, deviations far beyond the experimental uncertainty appear. Especially, the large deviations for the IPA potential are striking and might result from the fact that the IPA potential was reported with too few potential points.

The dissociation energies  $D_e$  referred to the minimum of the PECs and the dissociation energy  $D_0$  referred to the level  $v'' = 0, J'' = 0$  are gathered in Table V, together with the results from Ref. 16 for comparison. The averaged values have been calculated only from results of the models X, MLR, and TT, which use the same long-range parameters  $C_n$ . The idea that the large difference of the Chebychev model is mainly related to the different long-range behaviors is supported by the fact that the zero point energies given in the right column of Table V differ by less than  $0.02 \text{ cm}^{-1}$ , which is the experimental uncertainty. For estimating the uncertainty limit of the new value of  $D_e$  compared to the earlier one of Ref. 16, we use the

TABLE V. Dissociation energies derived by the different models for  $^{24}\text{Mg}_2$ . The averages are calculated only from the models X, MLR, and TT, which employ the same long-range parameters  $C_n$ . The uncertainties given for the averages of  $D_e$  and  $D_0$  include the standard deviation and the influence of the uncertainties of the long-range parameters given in Ref. 20 for  $C_6$  and  $C_8$ , assuming 10% uncertainty of  $C_{10}$ . For  $E(v'' = 0, J'' = 0)$ , we give the standard deviation.

Model	$D_e$ ( $\text{cm}^{-1}$ )	$D_0$ ( $\text{cm}^{-1}$ )	$E(v'' = 0, J'' = 0)$ ( $\text{cm}^{-1}$ )
X-rep.	430.472	405.233	25.239
TT	430.144	404.904	25.240
MLR	430.369	405.133	25.236
Chebychev	429.945	404.707	25.238
Ref. 16	430.1(1.0)	404.8 (1.0)	25.264
Averages of X, MLR, and TT	430.3(5)	405.1(5)	25.238(2)

extrapolation from the highest observed level to the asymptote through the long-range parameters  $C_6, C_8$ , and  $C_{10}$ <sup>19,20</sup> and their uncertainties of 2%, 1.2%, and 10% (assumed), respectively, and obtain  $0.5 \text{ cm}^{-1}$ , thus a slight improvement by a factor of two to Ref. 16. The difference of the zero point energy to the one calculated from the Dunham expansion in Ref. 16 is significant, it might be traced back to a different definition of this quantity.

We can now compare the experimentally determined dissociation energy  $D_e$  and vibrational frequency  $\omega_e = 51.286(19) \text{ cm}^{-1}$  (from X-representation) with the results of the latest *ab initio* calculations,<sup>17</sup>  $D_e = 404 \text{ cm}^{-1}$  and  $\omega_e = 45.4 \text{ cm}^{-1}$  for  $^{24}\text{Mg}_2$ . The differences for both properties are significant regarding the precision of spectroscopic work. However, the *ab initio* results are helpful guidelines especially for the spectroscopy and identification of excited electronic states.

The scattering length is very sensitive to the position of the last bound state relative to the dissociation limit, so we recalculated the scattering lengths because the value of  $431(1) \text{ cm}^{-1}$  used by Ref. 18 has changed to  $430.3(5)$ . The results are collected in Table VI.

The scattering length for the main isotopologue  $^{24}\text{Mg}_2$  agrees very well with the former determination by Tiesinga *et al.*<sup>18</sup> It behaves remarkably stable with respect to small changes of the potential resp. the dissociation energy, as can

TABLE VI. Scattering lengths derived from the different potential approaches. The results for the Chebychev model are not included in the average because its long-range behavior is different due the missing  $C_{10}$  contribution.

Potential model	Scattering length ( $\text{\AA}$ )		
	$^{24}\text{Mg}_2$	$^{25}\text{Mg}_2$	$^{26}\text{Mg}_2$
X-rep.	14.4	-130	28.2
MLR	14.6	-102	28.7
TT	16.0	-63	31.1
Avg.	15(3)	-100(40)	29(5)
Chebychev	21	-15	41
$^{24}\text{Mg}_2$ (Ref. 18)	14(5)		

also be seen by comparing the result of  $a = 21 \text{ \AA}$  from the Chebychev model. For the isotopologue  $^{25}\text{Mg}_2$ , the last bound level is lower in energy and leads to a large negative scattering length. This fact results to a significant sensitivity on small changes in the potential functions. For the isotopologue  $^{26}\text{Mg}_2$ , the potentials support an additional vibrational level,  $v = 19$  compared to  $v = 18$  for the others, which again results in a positive scattering length, about twice as large as the one of  $^{24}\text{Mg}_2$  and thus a bit more sensitive to the differences in potential functions.

The uncertainty of the long-range parameters (e.g.,  $C_6 \approx 2\%^{20}$ ) will contribute to the uncertainty of the scattering lengths. We have checked the effect of the 2% uncertainty in  $C_6$ .<sup>20</sup> It is the major contribution and yields a change  $\Delta a \leq 2 \text{ \AA}$  for  $^{24}\text{Mg}_2$ . Altogether, the uncertainty is estimated to be  $\Delta a \leq 3 \text{ \AA}$  for this atom pair and is contained in Table VI for the average. For the other cases, the total variations of the potentials will dominate the error limits.

We searched carefully for levels, which, when excited, would decay to high vibrational levels of  $X^1\Sigma_g^+$  but failed despite sufficiently large Franck-Condon factors. Calculation of transition probabilities beyond the Franck-Condon principle are needed and for that purpose good *ab initio* results on dipole transition moment functions. The ground state potential would support vibrational levels up to  $v'' = 18$  for  $^{24}\text{Mg}_2$ , but the last observed one is only  $v'' = 13$  resulting in an energy gap to the asymptote of  $20 \text{ cm}^{-1}$ .

Summing up, we have reported new and significantly improved spectral data of  $\text{Mg}_2$  and presented a set of potential models describing the ground state  $X^1\Sigma_g^+$ . All checked potential forms can be used for calculation of the studied bound levels with comparable accuracy. For extrapolation to the last bound levels and the atom pair asymptote, we recommend to use those forms, which have built in the proper long-range function, i.e., X-, MLR-, and TT-representation, assuming that the calculated long-range parameters are reliable. The scattering lengths for  $^{24}\text{Mg}_2$  and for  $^{26}\text{Mg}_2$  are positive, for the isotopologue  $^{25}\text{Mg}_2$  the value is large and negative resulting also in a larger uncertainty. Thus Bose-Einstein condensation should be in reach for the even isotopes. Photo association experiments such as for  $\text{Ca}^{35}$  and  $\text{Sr}^{36}$  would be highly desirable for obtaining the binding energies of the least bound levels.

## ACKNOWLEDGMENTS

The work is supported by the DFG through QUEST, the Centre for Quantum Engineering and Space-Time Research. We are grateful to Professor E. Rasel for the loan

of an UV-Ar+ laser and we thank Dr. M. Krosnicki for providing us with the lists of their *ab initio* PECs.<sup>17</sup> S.R. gratefully acknowledges financial support by E. Rasel and E.T. the support from the Minister of Science and Culture of Lower Saxony, Germany, by providing a Niedersachsenprofessur.

- <sup>1</sup>S. Kraft, F. Vogt, O. Appel, F. Riehle, and U. Sterr, *Phys. Rev. Lett.* **103**, 130401 (2009).
- <sup>2</sup>S. Stellmer, M. K. Tey, B. Huang, R. Grimm, and F. Schreck, *Phys. Rev. Lett.* **103**, 200401 (2009); Y. N. M. de Escobar, P. G. Mickelson, M. Yan, B. J. DeSalvo, S. B. Nagel, and T. C. Killian, *ibid.* **103**, 200402 (2009).
- <sup>3</sup>Y. Takasu, K. Maki, K. Komori, T. Takano, K. Honda, M. Kumakura, T. Yabuzaki, and Y. Takahashi, *Phys. Rev. Lett.* **91**, 040404 (2003).
- <sup>4</sup>J. Friebe, A. Pape, M. Riedmann, K. Moldenhauer, T. Mehlstäubler, N. Rehbein, C. Lisdat, E. M. Rasel, W. Ertmer, H. Schnatz, B. Lipphardt, and G. Grosche, *Phys. Rev. A* **78**, 033830 (2008).
- <sup>5</sup>O. Allard, C. Samuelis, A. Pashov, H. Knöckel, and E. Tiemann, *Eur. Phys. J. D* **26**, 155 (2003).
- <sup>6</sup>A. Stein, H. Knöckel, and E. Tiemann, *Eur. Phys. J. D* **57**, 171 (2010).
- <sup>7</sup>O. Allard, S. Falke, A. Pashov, O. Dulieu, H. Knöckel, and E. Tiemann, *Eur. Phys. J. D* **35**, 483 (2005).
- <sup>8</sup>A. Stein, H. Knöckel, and E. Tiemann, *Eur. Phys. J. D* **64**, 227 (2011).
- <sup>9</sup>D. Comparat, C. Drag, A. Fioretti, O. Dulieu, and P. Pillet, *J. Mol. Spectrosc.* **195**, 229 (1999).
- <sup>10</sup>K.-K. Ni, S. Ospelkaus, M. H. G. de Miranda, A. Pe'er, B. Neyenhuis, J. J. Zirbel, S. Kotochigova, P. S. Julienne, D. S. Jin, and J. Ye, *Science* **322**, 231 (2008).
- <sup>11</sup>H. Scheingraber and C. R. Vidal, *J. Chem. Phys.* **66**, 3694 (1977).
- <sup>12</sup>W. J. Balfour and A. E. Douglas, *Can. J. Phys.* **48**, 901 (1970).
- <sup>13</sup>W. C. Stwalley, *J. Chem. Phys.* **54**, 4517 (1971).
- <sup>14</sup>W. C. Stwalley, *Chem. Phys. Lett.* **7**, 600 (1970).
- <sup>15</sup>K. C. Li and W. C. Stwalley, *J. Chem. Phys.* **59**, 4423 (1973).
- <sup>16</sup>C. R. Vidal and H. Scheingraber, *J. Mol. Spectrosc.* **65**, 46 (1977).
- <sup>17</sup>E. Czuchaj, M. Krosnicki, and H. Stoll, *Theor. Chem. Acc.* **107**, 27 (2001).
- <sup>18</sup>E. Tiesinga, S. Kotochigova, and P. S. Julienne, *Phys. Rev. A* **65**, 042722 (2002).
- <sup>19</sup>S. G. Porsev and A. Derevianko, *Phys. Rev. A* **65**, 020701(R) (2002).
- <sup>20</sup>S. G. Porsev and A. Derevianko, *J. Exp. Theor. Phys.* **102**, 195 (2006).
- <sup>21</sup>E. J. Salumbides, K. S. E. Eikema, W. Ubachs, U. Hollenstein, H. Knöckel, and E. Tiemann, *Eur. Phys. J. D* **47**, 171 (2008).
- <sup>22</sup>F. James and M. Roos, *Minuit* (Cern library PACKLIB, 1989), p. D506.
- <sup>23</sup>R. J. LeRoy, *Can. J. Phys.* **52**, 246 (1974).
- <sup>24</sup>C. C. Lu, T. A. Carlson, F. B. Malik, T. C. Tucker, and C. W. Nestor, *At. Data Nucl. Data Tables* **3**, 1 (1971).
- <sup>25</sup>R. J. LeRoy, C. C. Haugen, J. Tao, and H. Li, *Mol. Phys.* **109**, 435 (2011).
- <sup>26</sup>K. T. Tang and J. P. Toennies, *J. Chem. Phys.* **66**, 1496 (1977).
- <sup>27</sup>K. T. Tang and J. P. Toennies, *J. Chem. Phys.* **68**, 5501 (1978).
- <sup>28</sup>K. T. Tang and J. P. Toennies, *J. Chem. Phys.* **80**, 3726 (1984).
- <sup>29</sup>K. T. Tang and J. P. Toennies, *Z. Phys. D* **1**, 91 (1986).
- <sup>30</sup>X. W. Sheng, P. Li, and K. T. Tang, *J. Chem. Phys.* **130**, 174310 (2009).
- <sup>31</sup>D. D. Yang, P. Li, and K. T. Tang, *J. Chem. Phys.* **131**, 154301 (2009).
- <sup>32</sup>G. P. Yin, P. Li, and K. T. Tang, *J. Chem. Phys.* **132**, 074303 (2010).
- <sup>33</sup>P. Li, W. Xie, and K. T. Tang, *J. Chem. Phys.* **133**, 084308 (2010).
- <sup>34</sup>L. Busevica, I. Klincare, O. Nikolayeva, M. Tamanis, R. Ferber, V. V. Meshkov, E. A. Pazyuk, and A. V. Stoljarov, *J. Chem. Phys.* **134**, 104307 (2011).
- <sup>35</sup>C. Degenhardt, T. Binnewies, G. Wilpers, U. Sterr, F. Riehle, C. Lisdat, and E. Tiemann, *Phys. Rev. A* **67**, 043408 (2003).
- <sup>36</sup>S. B. Nagel, P. G. Mickelson, A. D. Saenz, Y. N. Martinez, Y. C. Chen, T. C. Killian, P. Pellegrini, and R. Côté, *Phys. Rev. Lett.* **94**, 083004 (2005).